Chapter

Static Var Compensator with Fractional Order Dynamics for Enhanced Stability and Control

Nasim Ullah, Anwar Ali, Haider Ali, Asier Ibeas and Jorge Herrera

Abstract

This chapter presents a new theoretical approach for a novel static Var compensator (SVC) system using fractional order calculus. The thyristor-controlled reactor (TCR) and fixed capacitor are assumed to be noninteger. A state space model is derived for the fractional SVC and a novel fractional order sliding surface is proposed, based on which a fractional order controller is derived for bus voltage stabilization with variable loading. Keeping in view the enhanced stability margins of the system, the parameters of the control system are optimized using Simulink response optimization toolbox. The stability and the convergence proof of the control system is verified using fractional order Lyapunov theorem. The effectiveness of the proposed control scheme is verified using numerical simulations.

Keywords: static Var compensator, transmission line reactance, sliding mode controller, voltage stability, fractional inductor, fractional capacitor

1. Introduction

In recent times, the demand and the importance of a robust transmission network is increasing at an extraordinary rate. With the advancement of the society, it is vital to ensure the enough power availability to both the common consumer and the industry. The conventional transmission system has several disadvantages that include the lack of its operation on full load capacity, performance degradation under heavy inductive loads, and voltage sagging problems. Moreover, the conventional transmission system is not efficient in resolving and isolating the fault over the lines because most of the power systems are controlled through mechanical means. A more preferable alternative to the fixed mechanical control of the transmission network is the flexible AC transmission system (FACTS). All FACTS controllers are operated in a closed loop fashion and a detailed comparison of several control schemes is presented in the work given in [1].

The shunt compensators are preliminarily used for the reactive power compensation over the transmission network system. The reactive power is supplied or absorbed using the electronic drive-based shunt flexible ac transmission system (FACTS) controllers including the static Var compensator (SVC) and STATCOM [2, 3]. Over a transmission network bus voltage stability is a prime issue and it needs to be addressed for the overall stability of the power network. The bus voltage over

a transmission network is subject to the variations due to the stochastic nature of variable inductive load demands. The bus voltages are much dependent on the reactive power demands [3]. The utilization of the SVC as shunt compensation for voltage management and related concepts are discussed by the authors of reference [4]. SVC has a simple structure, which provides controlled reactive power compensation over the transmission network. Other shunt compensator such as static synchronous compensator (STATCOM), which is based on the power electronics converter concept, is an advanced version of the FACTS controllers [5]. The power electronics-based shunt compensator can provide dynamic stability of the power network over a wider range as compared to the conventional SVC-based system. However, the closed loop control structure in case of the power electronics-based FACTS controller is more complex as compared to the SVC. In [6], the authors proposed a coordinated control strategy for the dynamic stability of the SVC-based power network. In order to enhance the transient stability, damping of power oscillations, and economic operation of the power network, several researchers have proposed the utilization of the unified power flow controller (UPFC) that simultaneously provide the series and shunt compensation over the transmission network [7, 8]; however, the structure of the closed loop control system is very complex for the UPFC. Moreover, the solution is very costly as compared to the conventional SVC-based power system. Different applications of the UPFC and STACOM controllers in the power networks have been discussed in detail by the authors of Ref. [9–11]. Apart from the applications of the FACTS controllers, another important issue is to choose the optimal location for the installment of these controllers [12]. A detailed review on the optimal placement of the FACTS devices is presented in [13]. Apart from the benefits of the FACTS controllers, feedback system plays vital role in achieving the control objectives. Several integer order robust control methods have been proposed for the SVC-based power system control problem. The detailed discussion of the power flow stability using closed loop FACTS controllers are discussed by the authors of [14–17]. In the above cited work, the authors proposed several control techniques such as adaptive backstepping, fuzzy logic; Lyapunov-based nonlinear controller and the H∞ Control. In [18], the authors have proposed robust variable structure control system for the SVC-based power system. An important issue in the design of any control system is how to select the optimal parameters. Different approaches are used in the literature such as PSO-based parameters optimization [19] and genetic algorithm-based parameters selection in [20–24]. In [25, 26], two different variants of the robust controllers have been proposed for VSC-based HVDC system. Fractional calculus is finding numerous applications in the area of the modeling and control of the dynamic systems. Fractional order systems have some additional advantages over integer order systems such as high degree of freedom in the parameters selection, robustness to noise, offer less chattering in the control signal, and wide stability margins [27]. In [28, 29], the authors proved that the fractional order systems are stable even when the systems roots lie in the right half of the complex plane. The formulation of fractional order controllers based on fractional order models offer additional advantages such as reduced computational costs and more robustness against uncertainties [30, 31]. Several authors proposed fractional order model-based controllers such as robotic manipulators [32], thermal modeling of buildings [33], aircraft [34], and pneumatic actuators [35]. Based on the above literature survey, it is concluded that the wider stability region concepts of the fractional order systems can be applied in several fields of interests. Particularly, the fractional order dynamics can be introduced to the SVC-based power system dynamic systems for enhanced stability margins. Fractional order filters consisting of inductive and capacitive elements have been practically realized and discussed in the literature.

Fractional order tunable resonators and filters have been practically realized and the details are given in [36]. Electronically tunable all pass filter has been proposed and discussed in [37].

This chapter proposes static Var compensator (SVC) using fractional order inductive and capacitive elements. The idea is exploited theoretically and the dynamic equation of the fractional order susceptance is derived. Finally, a novel fractional order sliding surface is proposed and a feedback controller is derived for the bus voltage stabilization problem of power transmission network. The parameters of the proposed control scheme are tuned using Simulink response optimization tool box.

2. Mathematical model of TCR-FC type SVC by inclusion of fractional inductor and capacitor

Figure 1 shows the block diagram of the fractional order SVC-based power system. Before going into the details of the mathematical models of fractional order SVC, this section presents the definitions of the fractional calculus.

2.1 Definitions of fractional derivatives and integrals

Basic definition of the fractional operator can be denoted by a general fundamental operator ${}_aD_t^\alpha$ as a generalization of the differential and integral operators, and it is defined as [28].

$$ {}_aD_t^\alpha \cong D^\alpha = \begin{cases} \dfrac{d^\alpha}{dt^\alpha} & ,R(\alpha) > 0 \\ 1 & ,R(\alpha) = 0 \\ \int_a^t (d\tau)^{-\alpha} & ,R(\alpha) < 0 \end{cases} \tag{1} $$

Here α represents the order of fractional operator and $R(\alpha)$ represents set of real numbers. The following three definitions used for the general fractional operator are the Riemann–Liouville (RL) definition, the Caputo definition, and the Grunwald–Letnikov (GL) definition. The αth order Riemann–Liouville fractional derivative of function is given by [28].

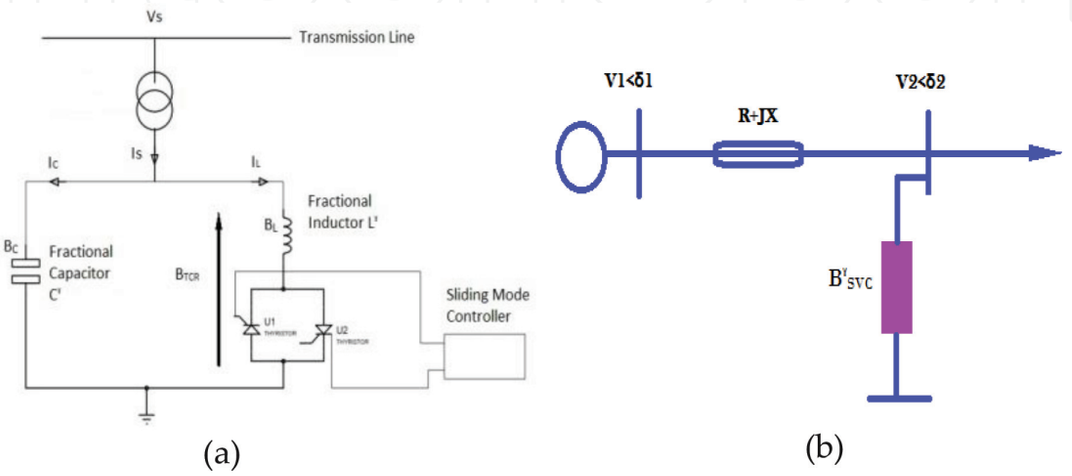

Figure 1.
(a) Configuration of fractional SVC (TCR-FC), (b) single machine infinite bus configuration.

$$ {}_aD_t^{\alpha} f(t) = \frac{d^{\alpha}}{dt^{\alpha}} f(t) = \frac{1}{\Gamma(m-\alpha)} \frac{d^m}{dt^m} \int_a^t \frac{f(\tau)}{(t-\tau)^{\alpha-m+1}} d\tau \tag{2} $$

Riemann–Liouville formula of the αth-order fractional integration can be written by

$$ {}_aD_t^{-\alpha} f(t) = I^{\alpha} f(t) = \frac{1}{\Gamma(\alpha)} \int_a^t \frac{f(\tau)}{(t-\tau)^{1-\alpha}} d\tau \tag{3} $$

Here m is the first integer larger than α, such that $m-1<\alpha<m$, with $t-a$ is the interval of integration and Γ is the Euler's Gamma function. The Caputo fractional derivative expression of a continuous function is expressed as

$$ {}_aD_t^{\alpha} f(t) = \begin{cases} \dfrac{1}{\Gamma(n-\alpha)} \displaystyle\int_a^t \frac{f^n(\tau)}{(t-\tau)^{\alpha-n+1}} d\tau & (n-1 \le \alpha < n) \\ \dfrac{d^n}{dt^n} f(t) & (\alpha = n) \end{cases} \tag{4} $$

The GL definition is given as:

$$ {}_a^{GL}D_t^{\alpha} f(t) = \lim_{h \to 0} \frac{1}{h^{\alpha}} \sum_{j=0}^{[(t-\alpha)/h]} (-1)^j \binom{\alpha}{j} f(t-jh) \tag{5} $$

Here, h represents the time step that is increasing with time and [.] is the integer part,

$$ \binom{\alpha}{j} = \frac{\Gamma(\alpha+1)}{\Gamma(j+1)\Gamma(\alpha-j+1)} \tag{6} $$

Theorem 1: *The following equation shows an autonomous system* [29]:

$$ {}_0D_t^{\alpha} x = Ax, \;\; x(0) = x_0 \tag{7} $$

Here α is differential order, $x \in R^n$ and $A \in R^{n \times n}$. The system is asymptotically stable if $|\arg(eig(A))| > \alpha\pi/2$. If the condition is satisfied then the system converges toward zero like $t^{-\alpha}$. The system stability is guaranteed if $|\arg(eig(A))| \ge \alpha\pi/2$ and the critical Eigen values that satisfy $|\arg(eig(A))| = \alpha\pi/2$ have geometric multiplicity. Moreover, the stable region of fractional system with $0 < \lambda < 1$ is larger than that of $1 < \lambda < 2$, $\lambda = 1$.

From **Figure 2**, it is clear that the fractional order systems with the fractional orders range of 0–1 have wider stability margins as compared to the integer order systems.

2.2 Mathematical model of fractional SVC-based power system

The goal of this work is to include the fractional components in the SVC mathematical model [18]. In order to modify the conventional design of TCR-FC type SVC, the fractional order inductor and capacitor are used to analyze and improve the system performance. Controllable part of the SVC is the susceptance, so the mathematical model derived in this section shall be represented in terms of the

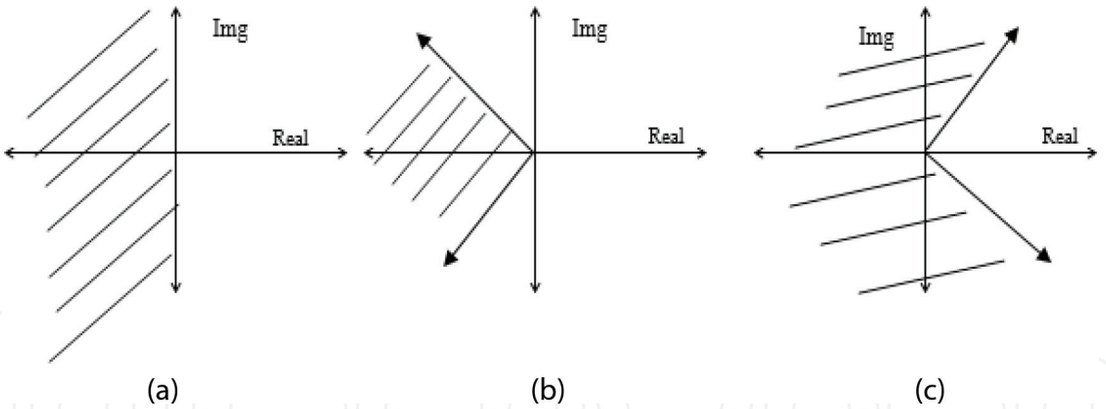

Figure 2.
Stability region of (a) integer order system (b) fractional order system with order between 1 and 2 (c) fractional order systems with order between 0 and 1.

susceptance (**B**). The block diagram of the system and single machine infinite bus configuration is shown in **Figure 1a** and **b**.

For the integer type of SVC-based power system, the expression of the susceptance is expressed as [18].

$$B_{SVC} = B_{TCR} + B_C \tag{8}$$

In Eq. (8), B_{TCR} represents the susceptance of the thyristor-controlled reactor and B_C is the susceptance of the fixed capacitor. The susceptance of the thyristor-controlled reactor depends on the degree of firing angle of the thyristor and it can be expressed as

$$B_{TCR} = \frac{B_L(2\pi - 2\alpha + \sin(2\alpha))}{\pi} \tag{9}$$

In Eq. (9), B_L represents the susceptance of the inductor. If the capacitor and inductor are noninteger, then Eq. (8) is expressed as

$$B_{SVCf} = B_{TCRf} + B_{Cf} \tag{10}$$

Here B_{SVCf} represents the fractional susceptance of the SVC configuration, B_{Cf} and B_{TCRf} represent the fractional susceptance of the inductive and capacitive elements. From Eq. (9), the fractional inductance of the inductor is expressed as B_{Lf} [31].

$$B_{Lf} = \frac{1}{2\pi f L_f} \tag{11}$$

The voltage dynamics across a fractional inductor is written as

$$\begin{pmatrix} \frac{D^\gamma I_L}{V_L} = \frac{1}{L_f} \\ L_f = \frac{V_L}{D^\gamma I_L} \end{pmatrix} \tag{12}$$

Combining Eqs. (12) and (11) yields the fractional order susceptance of the inductor as

$$B_{Lf} = \frac{1}{2\pi f \frac{V_L}{D^{\gamma} I_L}} \tag{13}$$

By multiplying the operator D^{γ} on both hand sides of Eq. (13) yields

$$D^{\gamma} B_{Lf} = D^{\gamma} \left[\frac{1}{2\pi f \frac{V_L}{D^{\gamma} I_L}} \right] \tag{14}$$

Using Eq. (14), and by equating $D^{\gamma} B_{Lf} = D^{\gamma} B_L$, Eq. (9) in fractional order sense is written as

$$B_{TCRf} = \frac{D^{\gamma} B_L (2\pi - 2\alpha + \sin(2\alpha))}{\pi} \tag{15}$$

The voltage and the current dynamics across the fractional capacitor is written as $V_c = \frac{1}{C_f} D^{-\gamma} I_c$. Here, V_c represents the voltage, I_c is the current across the capacitor, C_f is the fractional capacitance, and $D^{-\gamma}$ represents the fractional integrator. Now, the current–voltage dynamics across the fractional capacitor are expressed as [31].

$$C_f = \frac{I_c}{D^{\gamma} V_c} \tag{16}$$

The fractional capacitive susceptance is written as

$$\begin{pmatrix} B_{Cf} = 2\pi f C_f \\ B_{Cf} = 2\pi f \dfrac{I_c}{D^{\gamma} V_c} \end{pmatrix} \tag{17}$$

Simplifying Eq. (17) yields

$$D^{\gamma} B_{Cf} = 2\pi f D^{\gamma} \left(\frac{I_c}{D^{\gamma} V_c} \right) \tag{18}$$

By combining Eqs. (10), (15) and (18), one obtains

$$B_{SVCf} = \frac{D^{\gamma} B_L (2\pi - 2\alpha + \sin(2\alpha)) + \pi D^{\gamma} B_{Cf}}{\pi} \tag{19}$$

The modified state space representation of the power system with the fractional order SVC-based system configurations written as

$$\begin{aligned}
\dot{\delta} &= w \\
\dot{w} &= \frac{1}{M} \left(P_m - \frac{V_1 V_2 \sin\delta}{X} - Dw \right) \\
\dot{V}_2 &= \frac{1}{\tau} \left(\frac{-{V_2}^2}{X} + {V_2}^2 \left(\frac{D^{\gamma} B_L (2\pi - 2\alpha + \sin(2\alpha)) + \pi D^{\gamma} B_{Cf}}{\pi} \right) + \frac{V_1 V_2 \cos\delta}{X} - kP_d \right) \\
D^{\gamma} B_L &= \frac{1}{\tau} \left(V_{ref} - V_2 \right)
\end{aligned} \tag{20}$$

In Eq. (20), δ represents the power angle of the generator, w is the angular speed, P_m is the input mechanical power to the generator, D is the damping component, M is the moment of inertia, P_d represents the load demand over time, V_1 is the sending end voltage, and V_2 is the voltage over infinite bus.

3. Controller formulation and stability proof

The control objective is to formulate a robust control system for the fractional order SVC-based power system that must behave as insensitive to the disturbances and uncertainties, thus ensure a stabilized voltage over the transmission lines. Thus, the control objective is the regulation of the bus voltage V_2 regardless of the variation in the generation side and load side. Let $e = V_{2r} - V_2$, $\dot{e} = \dot{V}_{2r} - \dot{V}_2$ and the control signal is $B_{SVCf} = D^{\gamma}B_{SVC}$, then the fractional order sliding manifold is defined as

$$S = C_1 D^{-\alpha/2} e + C_2 \dot{e} \tag{21}$$

In the above expressions e represents the error signal, V_{2r} is the reference signal and $\dot{V}_2$ represents the first derivative of the command signal. Differentiating Eq. (21) with respect to D^{α} yields

$$D^{\alpha}S = C_1 D^{\alpha/2} e + C_2 D^{\alpha}\dot{e} \tag{22}$$

By combining Eqs. (20) and (22), one obtains

$$D^{\alpha}S = C_1 D^{\alpha/2} e + C_2 D^{\alpha}\left(\dot{V}_{2r} + \frac{1}{\tau}\frac{{V_2}^2}{X} - \frac{1}{\tau}{V_2}^2 D^{\gamma}B_{SVC} - \frac{V_1 V_2 \cos\delta}{\tau X} + \frac{1}{\tau}kP_d\right) \tag{23}$$

The control law is derived as

$$D^{\gamma}B_{SVC} = -\frac{\tau}{{V_2}^2}\left(-\frac{{V_2}^2}{\tau X} + \frac{V_1 V_2 \cos\delta}{\tau X} - \frac{k}{\tau}P_d - \dot{V}_{2r} - \frac{C_1}{C_2}D^{-\alpha/2}e - K_s D^{-\alpha}\mathrm{sgn}(S)\right) \tag{24}$$

The following inequality holds [30].

$$\left|\sum_{j=1}^{\infty}\frac{\Gamma(1+\alpha)}{\Gamma(1-j+\alpha)\Gamma(1+j)}D^{j}SD^{\alpha-j}S\right| \leq \tau|S| \tag{25}$$

Here τ is a positive constant. To prove the stability of the closed loop system, the Lyapunov function is chosen as $V = \frac{1}{2}S^2$. Applying operator D^{α} to the Lyapunov function yields

$$D^{\alpha}V = SD^{\alpha}S + \left|\sum_{j=1}^{\infty}\frac{\Gamma(1+\alpha)}{\Gamma(1-j+\alpha)\Gamma(1+j)}D^{j}SD^{\alpha-j}S\right| \tag{26}$$

Using Eq. (25), we can simplify Eq. (26) as

$$D^{\alpha}V \leq SD^{\alpha}S + \tau|S| \tag{27}$$

Using Eqs. (23) and (27), $D^{\alpha}V$ is calculated as

$$D^{\alpha}V \leq S\left(C_1 D^{\alpha/2}e + C_2 D^{\alpha}\left(\dot{V}_{2r} + \frac{1}{\tau}\frac{{V_2}^2}{X} - \frac{1}{\tau}{V_2}^2 D^{\gamma}B_{SVC} - \frac{V_1 V_2 \cos\delta}{\tau X} + \frac{1}{\tau}kP_d\right)\right) + \tau|S| \tag{28}$$

By combining Eqs. (24) and (28), one obtains

$$D^{\alpha}V \leq -K_s|S| + \tau|S| \tag{29}$$

The first term of Eq. (29) is negative, so if the discontinuous gain $K_S > |\tau|$, then it is shown that the fractional derivative of the Lyapunov function is always less than zero, that is, $D^{\alpha}V \leq 0$, which means that reaching condition of the sliding surface is satisfied and $S = 0$. The following lemmas are defined that will be used in the convergence proof.

Lemma 1*. If integral of the fractional derivative ${}_aD_t^{\alpha}$ of a function f(t) exists then according to* [30].

$${}_aD_t^{-\alpha}\left({}_aD_t^{\alpha}f(t)\right) = f(t) - \sum_{J=1}^{K}\left[{}_aD_t^{\alpha-J}f(t)\right]_{a=t}\frac{(t-a)^{\alpha-J}}{\Gamma(\alpha-J+1)} \tag{30}$$

Here $K-1 \leq \alpha < K$ and Γ represents the standard gamma function.

Lemma 2*. The fractional integral operator ${}_aD_t^{-\alpha}$ with $\alpha > 0$ is bounded such that the expression in Eq*. (31) *is valid* [29].

$$\left\|{}_aD_t^{-\alpha}f\right\|_P \leq K\|f\|_P; 1 \leq P \leq \infty; 1 \leq K \leq \infty \tag{31}$$

From Eq. (29) it is proved that the sliding surface is zero, that is, $S = 0$. With this condition Eq. (31) can be simplified as

$$\begin{bmatrix} D^{-\alpha/2}e = -\dfrac{C_2}{C_1}\dot{e} \\ D^{(1+\alpha/2)}e = -\dfrac{C_1}{C_2}e \end{bmatrix} \tag{32}$$

Multiplying Eq. (32) by $D^{-1-\alpha/2}$ and by further simplification, one obtains

$$\left\{\begin{array}{l} e = -\dfrac{C_2}{C_1}D^{-1-\alpha/2}e \\ D^{-\alpha/2}\left(D^{\alpha/2}e\right) = -\dfrac{C_2}{C_1}D^{-1-\alpha/2}e \end{array}\right\} \tag{33}$$

Using Lemma 1, Eq. (33) can be expressed as

$$e - \left[{}_{t_r}D_t^{(\alpha/2-1)}e\right]_{t=t_r}\frac{(t-t_r)^{\alpha/2-1}}{\Gamma(\alpha/2)} = -\frac{C_2}{C_1}D^{-1-\alpha/2}e \tag{34}$$

At time $t = t_r$, the term under the fractional integral of Eq. (34) is equal to zero, that is, $\left[{}_{t_r}D_t^{(\alpha/2-1)}e\right]_{t=t_r}\frac{(t-t_r)^{\alpha/2-1}}{\Gamma(\alpha/2)} = 0$, then the remaining expression of Eq. (34) can be written as

$$e = -\frac{C_2}{C_1}D^{-1-\alpha/2}e \tag{35}$$

Eq. (35) can be expressed as

$$D^{-2}D^{2}(e) = -\frac{C_2}{C_1}D^{-1-\alpha/2}e \tag{36}$$

Using Lemma 1, Eq. (36) is expanded as

$$e(t) - \left[{}_{t_r}D_t^{(2-1)}e(t)\right]_{t=t_r}\frac{(t-t_r)^{2-1}}{2} - e(t_r) = -\frac{C_2}{C_1}D^{-1-\alpha/2}e(t) \tag{37}$$

Application of Lemma 2 to the right hand side of Eq. (37) yields

$$-\frac{C_2}{C_1}D^{-1-\alpha/2}e(t) \leq -\frac{C_2}{C_1}K\|e(t)\| \tag{38}$$

Combination of Eqs. (37) and (38) yields

$$\|e(t) - \left[{}_{t_r}D_t^{(1)}e(t)\right]_{t=t_r}\frac{(t-t_r)}{2}\| - \|e(t_r)\| \leq -\frac{C_2}{C_1}K\|e(t)\| \tag{39}$$

If $S(t=t_s)=0$ and $e(t)=0$, then the necessary condition of convergence is $t_r \leq t_s < \infty$. Using this concept Eq. (39) can be expressed as

$$\left\{\begin{array}{l}\left[{}_{t_r}D_t^{(1)}e(t)\right]_{t=t_r}(t_s-t_r)\| \leq 2\|e(t_r)\| \\ \|[\dot{e}(t)]_{t=t_r}(t_r-t_s)\| \leq -2\|e(t_r)\|\end{array}\right\} \tag{40}$$

From Eq. (40), one obtains

$$t_r \leq t_s - \frac{2\|e(t_r)\|}{\|[\dot{e}(t)]_{t=t_r}\|} \tag{41}$$

From Eq. (41), it is proved that the error will converge near to the equilibrium points in finite time.

4. MATLAB/Simulink response optimization tool box

MATLAB/Simulink offers built-in response optimization tool box, which is extensively used for the optimal parameters selection of the control system [38]. To start the GUI, go to analysis tab of the simulink and click response optimization tool box. Define the parameters to be optimized in the MATLAB workspace. Then, use the response optimization tool box for importing the workspace defined parameters as design variables. The minimum and maximum search space of the design variables are adjusted. In the second step, the input reference signal is defined and imported using the toolbox. Finally, the output signal is imported from the simulink model that will follow the reference imported signal such that the error between the two signals is minimum. The error is minimized in an iterative manner and in this case, the error signal is the cost function. While minimizing the cost function, the parameters of the control system are adjusted online. The toolbox is associated with different optimization methods such as pattern search, simplex search, and gradient descent methods [39, 40].

5. Optimization of the control system for fractional order SVC-based system

The derived fractional order control system is shown in Eq. (24). For best control performance, it is vital to choose the optimal control parameters. This work compares the performance of the proposed controller (Eq. 24) to the conventional PID control system. The parameters of the proposed control scheme are optimized using Latin Hypercube method and Simulink response optimization toolbox. The order of the fractional operator is chosen constant as $\alpha = 0.8$.

To optimize the parameters, the cost function chosen is the integral of square of the error (ISE) between the reference command and the feedback signal. The initial values of the controller parameters are chosen as $C_1 = 0.58$, $C_2 = 0.78$, and $K_s = 0.48$. The convergence of the parameters to the optimal values is shown in **Figure 3**. The optimal parameters after convergence of the optimization algorithm are: $C_1 = 0.35$, $C_2 = 0.86$ and $K_s = 0.625$. The optimized step response of the closed system is shown in **Figure 4**.

The step response and optimized parameters of the PID controllers are shown in **Figures 5** and **6**. **Figure 5** shows the response of the system with optimized PID under nominal conditions. The optimal parameters are given in the table of **Figure 6**.

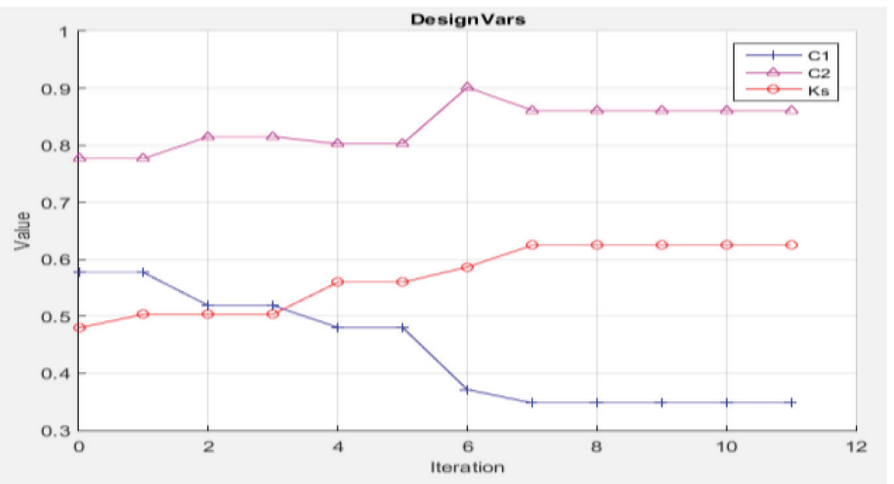

Figure 3.
Optimized parameters of the proposed scheme.

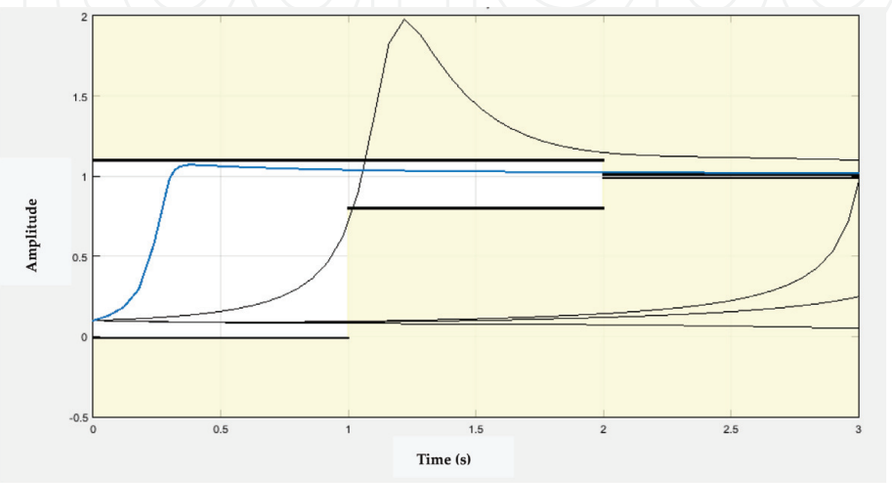

Figure 4.
Step response optimization.

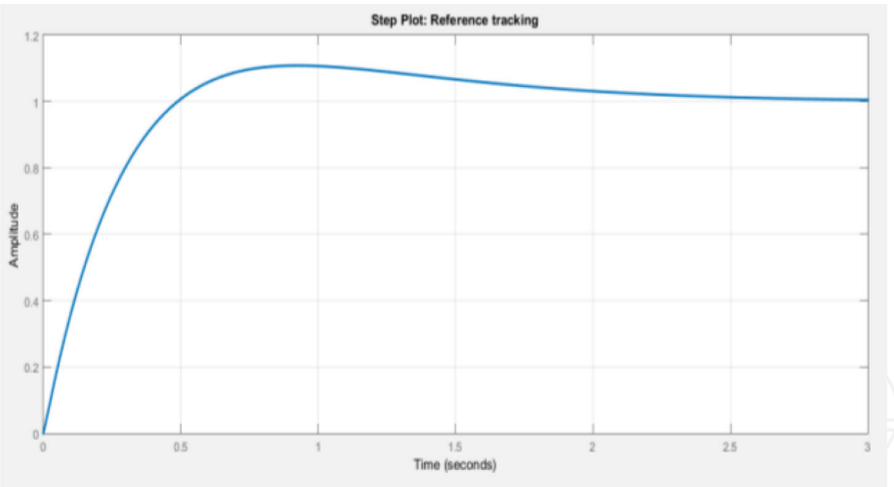

Figure 5.
PID step response optimization.

Controller Parameters

	Tuned	Block
P	34.3251	34.3251
I	42.0095	42.0095
D	-0.067456	-0.067456
N	508.8486	508.8486

Performance and Robustness

	Tuned	Block
Rise time	0.348 seconds	0.348 seconds
Settling time	2.27 seconds	2.27 seconds
Overshoot	10.9 %	10.9 %
Peak	1.11	1.11
Gain margin	Inf dB @ Inf rad/s	Inf dB @ Inf rad/s
Phase margin	77.4 deg @ 4.45 rad/s	77.4 deg @ 4.45 rad/s
Closed-loop stability	Stable	Stable

Figure 6.
Parameters of the optimized PID controller.

6. Results and discussions

For numerical simulations, the nominal parameters of the power system including the SVC configuration are given as following [18]: $M = 1$, $X = 0.5$, $V_1 = 1$, $\tau = 8$, $k = 0.25$, $D = 0.1$, and $P_m = P_d$. The Simulink simulation setup is shown in **Figure 7** and the profile of the load demand is shown in **Figure 8**.

6.1 Step response comparison

The control performance of the SVC-based power system under the step response is compared in **Figure 9**. The comparison is done for the error of the bus voltage stabilization response under the proposed fractional order control system and optimized PID. From the simulation results, it is concluded that the proposed

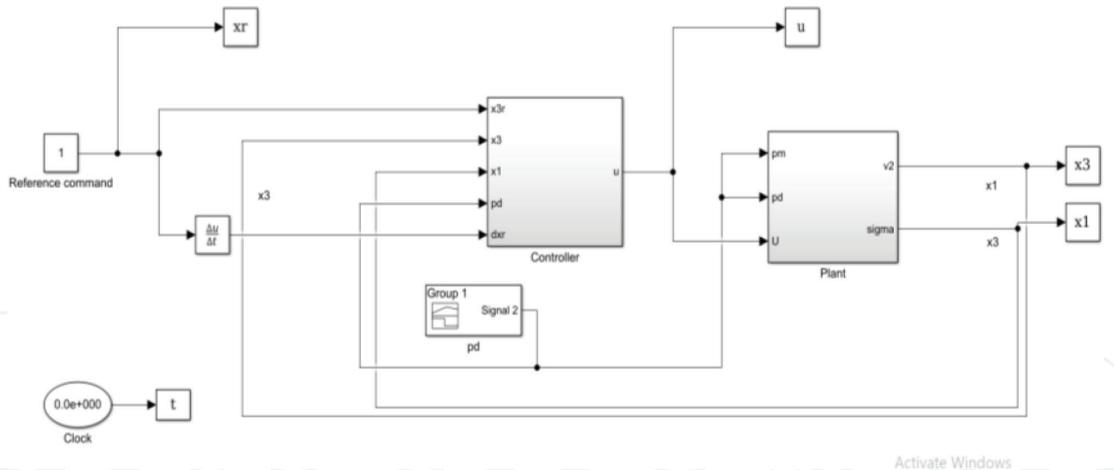

Figure 7.
MATLAB/SIMULINK simulation setup.

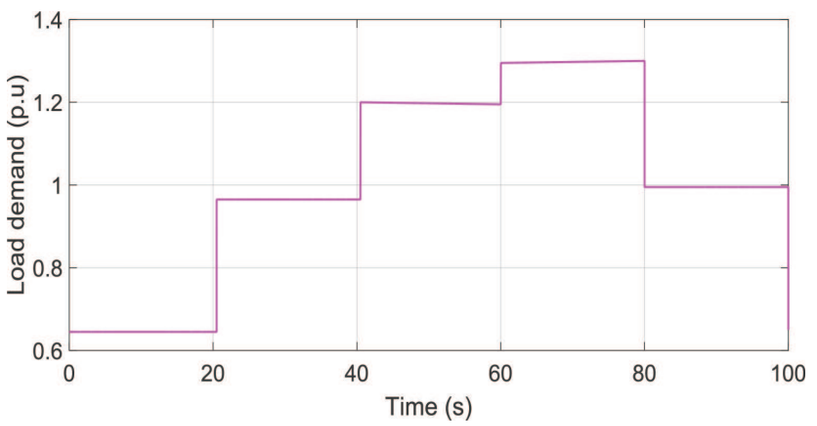

Figure 8.
Load demand profile.

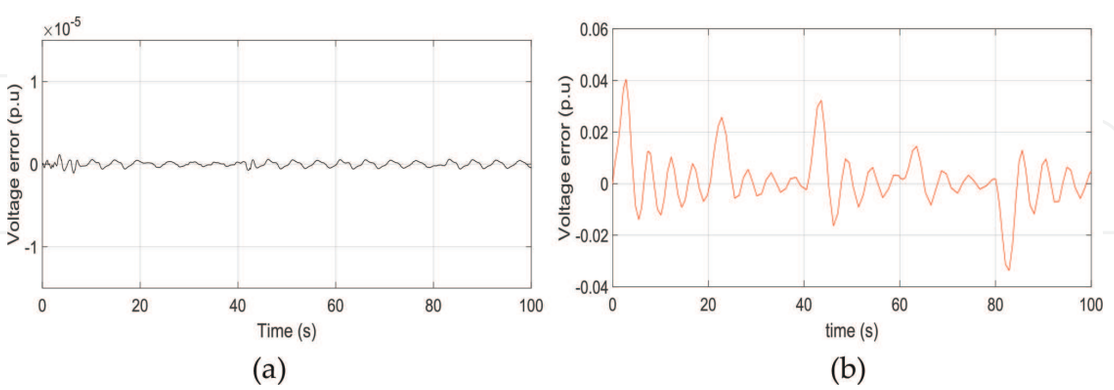

Figure 9.
Step response error (a) proposed scheme (b) optimized PID.

control system is more robust against the load demand variation profile as compared to the optimized PID control system.

6.2 Tracking response comparison

In this section, the bus voltage tracking performance of the SVC-based power network is compared under the action of the proposed control and the optimized

PID. The comparative results are shown in **Figure 10**. From the results provided, it is clear that the system under the proposed control scheme perfectly tracks the reference command while the system under the PID controller exhibits tracking errors of considerable magnitudes.

6.3 Performance comparison under inductive variable loading condition

The system's bus voltage stabilization under heavy inductive loads is compared under the action of the proposed control and the optimized PID. The simulation results are shown in **Figure 10**. The inductive load is varied gradually from time t = 60 sec and increased step wise till t = 100 sec. The proposed controller is robust against the dynamics introduced due to the heavy inductive loads. From **Figure 11**, it is clear that the response of the power system with PID-based SVC system suffers from voltage sage condition. The proposed controller-based SVC system is efficient in handling the situation and thus, the bus voltage error is very small with no voltage dips.

The control signals comparison is given in **Figure 12**. The proposed control system offers low frequency oscillations, which shows the robustness of the proposed method as compared to the PID method. Usually, in classical sliding mode control method, the robust term excites high frequency oscillations. Due to the high frequency oscillations, the classical sliding mode control is not feasible for practical

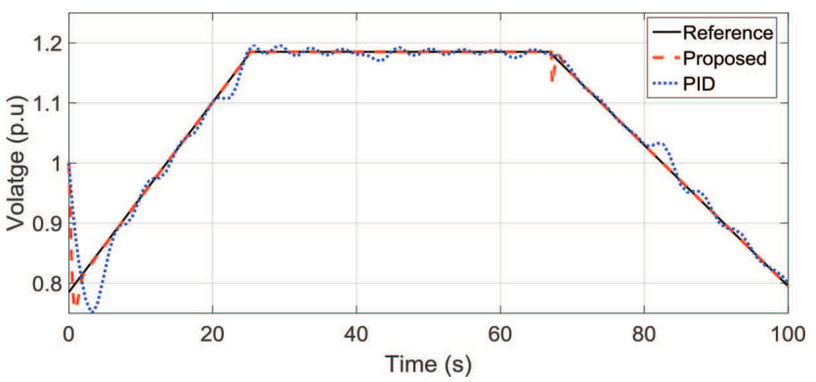

Figure 10.
Tracking response (a) proposed scheme (b) optimized PID.

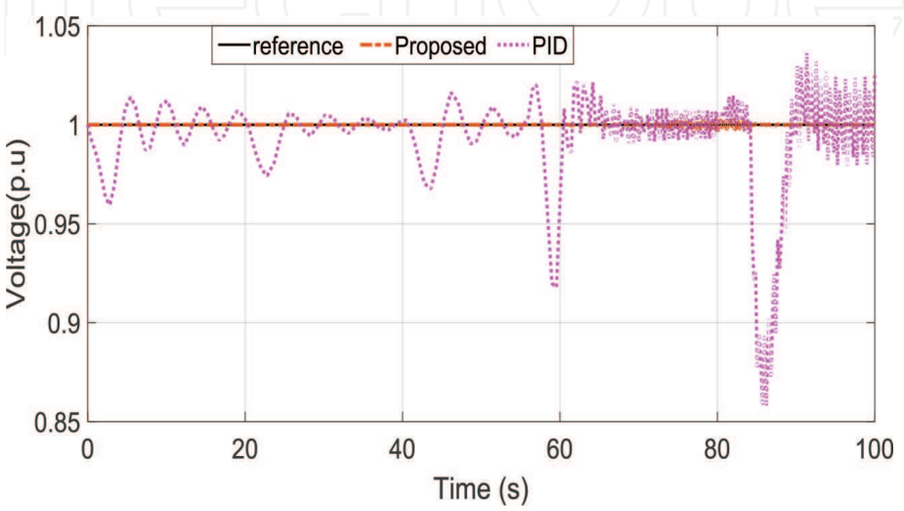

Figure 11.
Step response under heavy inductive loads (a) proposed scheme (b) optimized PID.

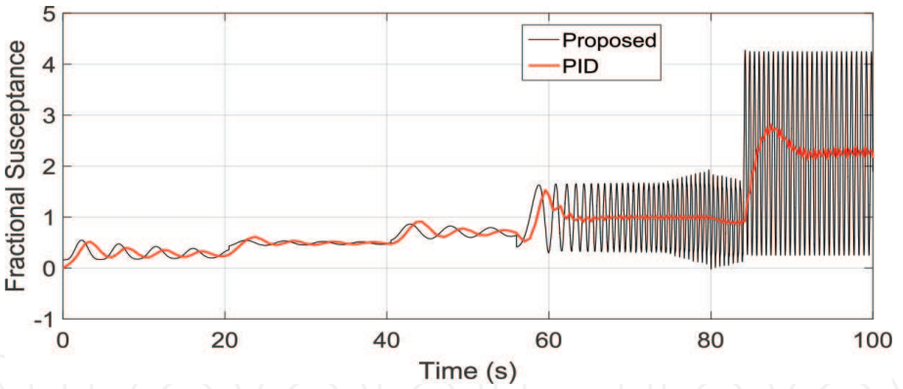

Figure 12.
Control signal comparison.

implementations. The proposed control method is noninteger in nature and from the control law given in Eq. (24), there is an integral term around the robust term, that is, signum function. So, it excites low frequency oscillations and thus it is very feasible for practical implementation over the microprocessor.

7. Conclusions

In this chapter, a fractional order SVC-based power system is discussed. Based on the fractional sliding manifold, a fractional order sliding control system is proposed. The robustness of the proposed control system is tested under the variable load demand and heavy inductive loading. The performance of the proposed control system is compared with a classical PID control system. From the results and discussion section, it is clear that the proposed control system is more robust as compared to the classical PID control under nonlinear loading profile. Moreover, the control chattering phenomenon is significantly reduced. The proposed control system is feasible for practical implementations.

Acknowledgements

The authors are thankful to the University of Technology Nowshera, Pakistan for providing the financial support for the publication of this chapter.

Author details

Nasim Ullah[1*], Anwar Ali[1], Haider Ali[1], Asier Ibeas[2] and Jorge Herrera[3]

1 University of Technology, Nowshera, Pakistan

2 Escola d'Enginyeria, Autonomous University of Barcelona, Barcelona, Spain

3 Departamento de Ingeniería, Universidad de Bogotá Jorge Tadeo Lozano, Bogotá, Colombia

*Address all correspondence to: nasim.ullah@uotnowshera.edu.pk

References

[1] Ma Y, Zhao T, Zhou X. An overview on control methods used in static var compensator. IEEE International Conference on Mechatronics and Automation (ICMA), Beijing; 2015. pp. 92-97. DOI: 10.1109/ICMA.2015.7237463

[2] Elmoudi R, Grinberg I, Safiuddin M. Design and implementation of static VAR compensator for classroom and research applications in smart grid laboratory. In: International Conference on Smart Grid (SGE), Oshawa, ON; 2012. pp. 1-8. DOI: 10.1109/SGE.2012.6463976

[3] Joshi BS, Mahela OP, Ola SR. Reactive power flow control using static VAR compensator to improve voltage stability in transmission system. In: International Conference on Recent Advances and Innovations in Engineering (ICRAIE), Jaipur; 2016. pp. 1-5. DOI: 10.1109/ICRAIE.2016.7939504

[4] Chopade P, Bikdash M, Kateeb I, Kelkar AD. Reactive power management and voltage control of large transmission system using SVC (static VAR compensator). In: Southeastcon, 2011 Proceeding of IEEE, Nashville, TN; 2011. pp. 85-90. DOI: 10.1109/SECON.2011.5752911

[5] Beza M. Power system stability enhancement using shunt-connected power electronic devices with active power injection capability. ISBN 978-91-7597-139-1 C MEBTU BEZA; 2015

[6] Wang CL, Hill Y. Transient stability and voltage regulation enhancement via coordinated control of generator excitation and SVC. International Journal of Electrical Power and Energy Systems. 2005;**27**(2):121-130

[7] Bhattacharyya B, Kumar Gupta V, Kuma S. UPFC with series and shunt FACTS controllers for the economic operation of a power system. Ain Shams Engineering Journal. September 2014; **5**(3):775-787

[8] Darwish MK, El-Habrouk M, Kasikci I. EMC compliant harmonic and reactive power compensation using passive filter cascaded with shunt active filter. EPE Journal. 2002;**12**(3):43-50. DOI: 10.1080/09398368.2002.11463511

[9] Banaei MR, Seyed-Shenava SJ, Farahbakhsh P. Dynamic stability enhancement of power system based on a typical unified power flow controllers using imperialist competitive algorithm. Ain Shams Engineering Journal. September 2014;**5**(3):691-702

[10] Mihalic R, Zunko P, Povh D. Improvement of transient stability using unified power flow controller. IEEE Transactions on Power Delivery. 1996; **11**(1):485-491

[11] Gupta S, Tripathi RK. Transient stability enhancement of multimachine power system using robust and novel controller based CSC-STATCOM. Advances in Power Electronics. 2015; **2015**:12. Article ID:626731. DOI:10.1155/2015/626731

[12] Albatsh FM, Ahmad S, Mekhilef S, Mokhlis H, Hassan MA. Optimal placement of unified power flow controllers to improve dynamic voltage stability using power system variable based voltage stability indices. PLoS One. 2015;**10**(4):e0123802. DOI: 10.1371/journal.pone.0123802

[13] Lavanya KSL, Sobha Rani P. A review on optimal location and parameter settings of FACTS devices in power systems. Era: Models, methods. International Journal for Modern Trends in Science and Technology. 2016;**02**(11): 112-117

[14] Sun LY, Tong S, Liu Y. Adaptive backstepping sliding mode H∞ control of static var compensator. IEEE Transactions on Control Systems Technology. Sept. 2011;**19**(5):1178-1185. DOI: 10.1109/TCST.2010.2066975

[15] Hemeida AM, Alkhalaf S, Alfarraj O. Control quality assessment of fuzzy logic controller based static VAR compensator (SVC). SAI Intelligent Systems Conference (IntelliSys), London. 2015;**2015**:507-517. DOI: 10.1109/IntelliSys.2015.7361187

[16] Fazal R, Choudhry MA. Design of non-linear static var compensator based on synergetic control theory. Electric Power Systems Research. 2017 October; **151**:243-250

[17] Safa A, Sakhaeifar M. Mismatched disturbance attenuation control for static var compensator with uncertain parameters. International Journal of Electrical Power and Energy Systems. 2017;**91**:61-70. ISSN: 0142-0615

[18] Kose E, Kizmaz H, Abaci K, Aksoy S. Control of SVC based on the sliding mode control method. Turkish Journal of Electrical Engineering and Computer Science; **22**(30):605-619

[19] Halacli MG, Demiroren A. Robust voltage/VAR control using PSO based STATCOM: A case study in Turkey. Journal of Electric Power Components and Systems. 2016;**44**(8):894-902

[20] Dulau M, Bica D. Design of robust control for single machine infinite bus system. Procardia Technology. 2015;**19**: 657-664

[21] Janaki M, Thirumalaivasan R, Prabhu N. Design of robust controller for VSC based HVDC using genetic algorithm. Advances in Electrical Engineering (ICAEE), 2014 International Conference on, Vellore. 2014:1-6. DOI: 10.1109/ICAEE. 2014.6838495

[22] Al Hamouz Z, Al Duwaish HN. A new load frequency variable structure controller using genetic algorithms. Electric Power Systems Research. 2000; **55**:1-6

[23] Al Musabi N, Al Hamouz Z, Al Duwaish H, Al Baiyat S. Variable structure load frequency controller using particle swarm optimization technique. In: Proceedings of the 10th IEEE International Conference on Electronics, Circuits and Systems; 2003. pp. 380-383

[24] Al Hamouza Z, Al Duwaisha H, Al Musabib N. Optimal design of a sliding mode AGC controller: Application to a nonlinear interconnected model. Electric Power Systems Research. 2011;**81**:1403-1409

[25] Nayak N, Routray SK, Rout PK. A robust control strategies to improve transient stability in VSC-HVDC based interconnected power systems. Energy, Automation, and Signal (ICEAS), 2011 International Conference on Bhubaneswar, Odisha; 2011. pp. 1-8. DOI: 10.1109/ICEAS.2011.6147186

[26] Nayak N, Routray SK, Rout PK. State feedback robust H∞ controller for transient stability enhancement of Vsc-Hvdc transmission systems. Procedia Technology. 2012;**4**:652-660

[27] Chen YQ, Petras I, Xue D. Fractional order control–A tutorial. In: 2009 American Control Conference Hyatt Regency Riverfront, St. Louis, MO, USA; June 2009. pp. 10-12

[28] Choudhary SK. Stability and performance analysis of fractional order control systems. Wseas Transactions on Systems and Control. 2014;**9**:438-444

[29] Area I, Batarfi H, Losada J, Nieto JJ, Shammakh W, Torres A. On a fractional order Ebola epidemic model. Advances in Difference Equations. 2015;**2015**:278. DOI: 10.1186/s13662-015-0613-5

[30] Efe MO. Fractional fuzzy adaptive sliding-mode control of a 2-DOF direct-drive robot arm. IEEE Transactions on in Systems, Man, and Cybernetics, Part B: Cybernetics. 2008;**38**(6):1561-1570. DOI: 10.1109/TSMCB.2008.918227

[31] Moreles MA, Lainez R. Mathematical modeling of fractional order circuits. arXiv: 1602.03541v121. Jan 2016

[32] Mujumdar A, Tamhane B, Kurode S. Fractional order modeling and control of a flexible manipulator using sliding modes. In: 2014 American Control Conference, Portland, OR; 2014. pp. 2011-2016. DOI: 10.1109/ACC.2014.6858955

[33] Lin C, Basu B, McCabe D. Fractional order models for system identification of thermal dynamics of buildings. Energy and Buildings. December 2016; **133**(1):381-388

[34] Ijaz S, Yan L, Humayun MT. Fractional order modeling and control of dissimilar redundant actuating system used in large passenger aircraft. Chinese Journal of Aeronautics. May 2018;**31**(5):1141-1152

[35] Razminia A, Baleanu D. Fractional order models of industrial pneumatic controllers. Abstract and Applied Analysis. 2014;**2014**:9. ID 871614. DOI: 10.1155/2014/871614

[36] Adhikary A, Sen S, Biswas K. Practical realization of tunable fractional order parallel resonator and fractional order filters. IEEE Transactions on Circuits and Systems I: Regular Papers. August 2016;**63**(8): 1142-1151. DOI: 10.1109/TCSI.2016.2568262

[37] Verma R, Pandey N, Pandey R. Electronically tunable fractional order all pass filter. IOP Conference Series: Materials Science and Engineering. 2017;**225**:012229. DOI: 10.1088/1757-899X/225/1/012229

[38] Available from: https://www.mathworks.com/help/sldo/gs/optimize-controller-parameters-to-meet-step-response-requirements-gui.html

[39] Ullah N, Shaoping W, Khattak MI, Shafi M. Fractional order adaptive fuzzy sliding mode controller for a position servo system subjected to aerodynamic loading and nonlinearities. Aerospace Science and Technology. June 2015: 381-387

[40] Ullah N, Han S, Khattak MI. Adaptive fuzzy fractional-order sliding mode controller for a class of dynamical systems with uncertainty. Transactions of the Institute of Measurement and Control. 2015:1-12. DOI: 10.1177/0142331215587042